Comparison of a one-dimensional particle-in-cell–Monte Carlo model and a one-dimensional fluid model for a CH_4/H_2 capacitively coupled radio frequency discharge

Vladimir Ivanov, Olga Proshina,[a] Tatyana Rakhimova, and Alexander Rakhimov
Skobeltsyn Institute of Nuclear Physics, Moscow State University, Vorob'evi Gori, Moscow 119899, Russia

Dieter Herrebout and Annemie Bogaerts
Department of Chemistry, University of Antwerp, Universiteitsplein 1, B-2610 Wilrijk-Antwerp, Belgium

(Received 25 October 2001; accepted for publication 23 January 2002)

A one-dimensional particle-in-cell–Monte Carlo (PIC–MC) model was developed for a capacitively coupled rf discharge in a mixture of CH_4 and H_2. The electron behavior is kinetically simulated by solving Newton's equations and treating the electron collisions with the Monte Carlo algorithm, whereas the behavior of the ions and radicals is treated by a set of continuity equations. The distinctive feature of this model is its self-consistency, i.e., the motion of the electrons is considered in the real electric field calculated from the Poisson equation, and not in the time-averaged electric field. The PIC–MC results were compared with the data calculated by means of a pure fluid model. In both models, exactly the same type of species, reactions, and cross sections are used. The results of both models, such as the electron energy distribution function, the average electron energy, and the densities of the various plasma species, are compared at a gas pressure of 0.14 Torr and a discharge frequency of 13.56 MHz, for the power ranging from 0.5 to 25 W. The nonstationary and nonlocal features of the electron energy distribution function are shown in the PIC–MC calculations. The effect of accumulation of low-energy electrons in the center of the discharge at higher input power $P=25$ W is observed in the PIC–MC model, in contrast with the fluid model. The mechanisms causing the accumulation of low-energy electrons, and the processes defining the stationary state of the discharge are analyzed. The applicability of the fluid model for the calculation of the density of different hydrocarbon radicals is discussed. [DOI: 10.1063/1.1461895]

I. INTRODUCTION

Capacitively coupled rf discharges in a mixture of CH_4/H_2 are frequently used for the deposition of diamond-like carbon (DLC) layers, by plasma-enhanced chemical vapor deposition.[1–3] In order to improve the results of the DLC deposition (i.e., film quality, deposition rate, film uniformity) as well as to explore the possibilities of up-scaling to larger reactors, a good insight into the plasma is desirable. This can be obtained by numerical modeling. In the literature, there exist a number of models for CH_4/H_2 plasmas.[1,3–12] Most of them are based on the fluid approach, but they can be distinguished from each other in the way they treat the electron kinetics by using constant electron reaction rate coefficients,[4,5] by using these rate coefficients as fitting parameters,[6] or by assuming a Druyvensteyn-like[7,8] or a Maxwellian[11] electron energy distribution function (EEDF) to calculate the electron reaction rate coefficients. Alternatively, the reaction rate coefficients can also be obtained as a function of the average electron energy, by means of the Boltzmann equation using the two-term approximation.[1,12] This method is the most accurate one of the fluid approaches found in the literature. However, the average electron energy in the fluid model is then still calculated by the electron energy balance equation in the local field approximation, and this method might not be valid at low pressures typically used for plasma-enhanced chemical vapor deposition of DLC films. A more accurate approach would be to handle the electrons in a fully kinetic way, by following their trajectory in the plasma by Newton's equations of motion, and by treating the collisions with the Monte Carlo algorithm. The self-consistent description of the electron behavior with the behavior of the molecules, ions, and radicals, and with the solution of Poisson's equation for the electric field distribution, leads to the particle-in-cell–Monte Carlo (PIC–MC) method.

Effective PIC–MC algorithms were applied for modeling low-pressure rf discharges in rare gases and in molecular gases (e.g., H_2, SiH_4).[13–19] A one-dimensional (1D) PIC–MC simulation for a rf discharge in methane was developed by Nagayama *et al.*[20] Usually PIC–MC models consider 10^5-10^6 superparticles and take considerable computing time. In order to get stable results with a relatively smaller number of particles and to reduce the computational efforts, a time-averaging technique was used.[20] Since the data were averaged over a larger number of rf periods, this method did not allow us to obtain a real time-dependent solution. Besides a simplified model of the plasma–chemical kinetics was used in that work, e.g., no electron-impact excitation reactions were taken into account. Since in reality a consid-

[a]Author to whom correspondence should be addressed; electronic mail: oproshina@mics.msu.su

TABLE I. Different species taken into account in the model beside electrons.

Neutral		Ions			Radicals	
CH_4	H_2	CH_4^+	CH_3^+	H_2^+	C_2H_5	CH_3
C_2H_6	C_3H_8	CH_5^+	$C_2H_5^+$	H_3^+	CH_2	CH
C_2H_4	C_2H_2	$C_2H_4^+$	$C_2H_2^+$	⋯	H	⋯

erable fraction of the electron energy is lost in vibrational excitation reactions,[12] the results[20] cannot be compared adequately with the other models and experimental data.

In the present article, we have developed a time-dependent 1D PIC–MC model for a CH_4/H_2 capactively coupled rf discharge and we will compare the calculation results with the results obtained from the 1D fluid model.[12] In Sec. II, the chemical (fluid) model and the PIC–MC approach will be outlined. Section III deals with the comparison of both models, and the conclusions are given in Sec. IV.

II. DESCRIPTION OF THE MODEL

A. Chemical model

The chemical model was presented in detail elsewhere,[12] and therefore it will only briefly be outlined here. There are 21 species (electrons, ions, radicals, and background molecules) considered in this model, as is illustrated in Table I. It is important to note that higher order neutral molecules (such as C_2H_6, C_3H_8, C_2H_4, and C_2H_2) are also included in the model, because it is stated in the literature that they can have rather high densities in the plasma.[3,9] Furthermore, it should be mentioned that negative ions (mainly CH_2^- and H^-) are not incorporated in the model, because it is found[1] that a CH_4 plasma has a strong electropositive character.

The total set of the chemical reactions taken into account in the model is given in Table II. For the ion–neutral and neutral–neutral reactions, constant reaction rate coefficients are assumed, and the values are given in Table II. The rate coefficients of electron–neutral reactions were calculated by using appropriate cross sections as a function of the electron energy and the EEDF. In the PIC–MC model, the EEDF was calculated directly, which allowed us to take into account the effects of nonlocality and time dependency. In the fluid model, a Boltzmann solver with the two-term approximation was used to calculate the EEDF in the local field approximation. The results of this calculation were presented in the form of a table in which the rate coefficient of every electron–neutral reaction is a function of the average electron energy. These tables are then used as input in the fluid code. In combination with the average electron energy as calculated by the electron energy balance equation, the electron–neutral reaction rates can be obtained. In the PIC–MC model these rates were obtained directly through the MC simulation of the electron (trajectories) collisions.

Based on these reactions, a number of continuity equations (one for each type of species) is constructed with different production and loss terms:

$$\frac{\partial n_i}{\partial t} = -\frac{\partial \Gamma_i}{\partial z} + S_i(z,t), \tag{1}$$

TABLE II. Set of reactions taken into account ion our model.

Reaction	Rate coefficient (m^3/s)
Electron–neutral reactions	
$e^- + CH_4 \rightarrow CH_4^*(v) + e^-$	$f(\varepsilon)$[a]
$e^- + CH_4 \rightarrow CH_4^+ + 2e^-$	$f(\varepsilon)$[b]
$e^- + CH_4 \rightarrow CH_3^+ + H + 2e^-$	$f(\varepsilon)$[b]
$e^- + CH_4 \rightarrow CH_3 + H + e^-$	$f(\varepsilon)$[b]
$e^- + CH_4 \rightarrow CH_2 + 2H + e^-$	$f(\varepsilon)$[b]
$e^- + H_2 \rightarrow H_2^*(v) + e^-$	$f(\varepsilon)$[a]
$e^- + H_2 \rightarrow 2H + e^-$	$f(\varepsilon)$[b]
$e^- + H_2 \rightarrow H_2^+ + 2e^-$	$f(\varepsilon)$[b]
$e^- + C_2H_6 \rightarrow C_2H_6^*(v) + e^-$	$f(\varepsilon)$[a]
$e^- + C_2H_6 \rightarrow C_2H_4^+ + H_2 + 2e^-$	$f(\varepsilon)$[b]
$e^- + C_2H_6 \rightarrow C_2H_5 + H + e^-$	$f(\varepsilon)$[b]
$e^- + C_3H_8 \rightarrow C_3H_8^*(v) + e^-$	$f(\varepsilon)$[a]
$e^- + C_3H_8 \rightarrow C_2H_4 + H_2 + CH_4 + e^-$	$f(\varepsilon)$[b]
$e^- + C_2H_4 \rightarrow C_2H_4^*(v) + e^-$	$f(\varepsilon)$[a]
$e^- + C_2H_4 \rightarrow C_2H_4^+ + 2e^-$	$f(\varepsilon)$[b]
$e^- + C_2H_4 \rightarrow C_2H_2 + 2H + e^-$	$f(\varepsilon)$[b]
$e^- + C_2H_2 \rightarrow C_2H_2^*(v) + e^-$	$f(\varepsilon)$[a]
$e^- + C_2H_2 \rightarrow C_2H_2^+ + 2e^-$	$f(\varepsilon)$[b]
Ion–neutral reactions	
$CH_4^+ + CH_4 \rightarrow CH_5^+ + CH_3$	1.5×10^{-15}
$CH_3^+ + CH_4 \rightarrow C_2H_5^+ + H_2$	1.2×10^{-15}
$CH_5^+ + C_2H_6 \rightarrow C_2H_5^+ + CH_4 + H_2$	5.0×10^{-16}
$H_2 + H_2^+ \rightarrow H_3^+ + H$	2.5×10^{-15}
$H_3^+ + CH_4 \rightarrow CH_5^+ + H_2$	1.6×10^{-15}
$H_3^+ + C_2H_6 \rightarrow C_2H_5^+ + 2H_2$	2.0×10^{-15}
$H_3^+ + C_2H_4 \rightarrow C_2H_5^+ + H_2$	1.9×10^{-15}
Neutral–neutral reactions	
$CH_3 + CH_3 \rightarrow C_2H_6$	3.7×10^{-17}
$CH_3 + H \rightarrow CH_4$	7.0×10^{-18}
$C_2H_5 + H \rightarrow CH_3 + CH_3$	6.0×10^{-17}
$C_2H_5 + CH_3 \rightarrow C_3H_8$	4.2×10^{-18}
$CH_2 + H \rightarrow CH + H_2$	2.7×10^{-16}
$CH + CH_4 \rightarrow C_2H_5$	1.0×10^{-16}
$CH_2 + CH_4 \rightarrow CH_3 + CH_3$	1.7×10^{-17}
$CH_2 + CH_4 \rightarrow C_2H_4 + H_2$	1.7×10^{-17}
$CH_4 + CH \rightarrow C_2H_4 + H$	1.0×10^{-16}
$CH_3 + CH_2 \rightarrow C_2H_4 + H$	3.3×10^{-17}
$C_2H_5 + H \rightarrow C_2H_4 + H_2$	3.0×10^{-18}
$CH_2 + CH_2 \rightarrow C_2H_2 + H_2$	1.1×10^{-16}

[a]Vibrational excitation reactions were taken into account only in the EEDF calculations, and not in the kinetic model in order to limit number of species.

[b]The rate coefficients of electron–neutral reactions were calculated by using appropriate cross sections as a function of the electron energy ε and the EEDF.

where n_i is the density and Γ_i is the flux of particle i. The particle fluxes are calculated by the drift-diffusion approximation

$$\Gamma_i = -D_i \frac{\partial n_i}{\partial z} + n_i \mu_i E, \tag{2}$$

where μ_i and D_i are the mobility and diffusion coefficients, respectively.

Since the characteristic momentum transfer frequencies for the ions are comparable to the rf frequency, an effective electric field $E_{\text{eff},i}$[21] was taken to account to use the diffusion-drift approximation for ions:

$$\frac{\partial E_{\mathrm{eff},i}}{\partial t} = \nu_{m,i}(E - E_{\mathrm{eff},i}). \tag{3}$$

Here $\nu_{m,i}$ is the momentum transfer frequency for ion i.

The source term S_i represents the creation and destruction of the particles by electron impact collisions and by chemical reactions (see Table II). This term also takes into account the inlet of feedstock gases and the pumping in the deposition reactor in the approach of a good mixing.

The boundary condition for the equations is

$$\Gamma_i|_{z=0,L} = \frac{\beta_i}{1-\frac{\beta_i}{2}} \times \frac{n_i v_{t,i}}{4}\Bigg|_{z=0,L}, \tag{4}$$

where $v_{t,i}$ is the thermal velocity of particle i, and β_i is the surface loss probability on the electrode surface.

Our estimations show that in the conditions under consideration the drift-diffusion approximation is correct for the description of the ion motion in the effective electric field in the bulk plasma and presheaths, whereas the correctness of this approximation cannot be justified accurately for the sheaths. Really, the ion scattering length may exceed the sheath length. The correct description of the ion acceleration in the sheaths should include kinetic simulation of the ion behavior. It may essentially influence the energy of incident ions on the substrate, which is very important for heterogeneous processes such as DLC film deposition. We did not consider such processes in this article, focusing on the processes in the bulk plasma. That is why we used the simple drift-diffusion approximation for ion motion, which can give only qualitative results in the sheath layers.

The total pressure p_{tot} in the reactor is given by the ideal gas law

$$p_{\mathrm{tot}} = k_b T_g \sum n_i, \tag{5}$$

where k_b is the Boltzmann constant and T_g is the gas temperature.

These continuity equations are coupled to Poisson's equation for a self-consistent solution of the electric field distribution (also see Sec. II B). More information about the reactions taken into account, their rate coefficients, as well as about the transport coefficients of ions and radicals, can be found in Herrebout *et al.*[12]

B. PIC–MC model

In order to describe accurately the nonlocal electron behavior, a PIC–MC model is used to follow the electrons. This method consists of integrating the equations of motion for a number of superelectrons. Every superelectron is composed of a large number of real electrons, moving with the same velocity. In the 1D model, the equations of motion take the form

$$m\frac{d^2z}{dt^2} = eE(z,t), \quad m\frac{d^2x}{dt^2} = 0, \quad m\frac{d^2y}{dt^2} = 0. \tag{6}$$

To solve the equations, a second order finite-difference scheme was used. The electron density n_e, which is used later in solving the Poisson equation, is determined by linear interpolation according to the new locations of the superelectrons and the superelectron sizes. The electron wall reflection ratio is set equal to zero, i.e., each superelectron is removed from the model when it reaches the walls.

During each time step, every superelectron may particulate in one of the electron–neutral processes given in Table II. The probabilities of the processes are evaluated by the formula

$$W = N v \sigma \, dt, \tag{7}$$

where N is the density of the target species, v is the electron velocity, σ is the cross section of the processes, and dt is the time step. The electron impact cross sections are taken the same as in Herrebout *et al.*[12] The energy loss of electrons with energy ε and mass m due to elastic collisions with molecules of mass M is calculated by $\Delta\varepsilon = 2m/M\varepsilon$. The electron energy loss due to inelastic collisions was equal to the excitation energy or ionization potential. The sum of the energy of the primary and secondary electrons, which are formed after ionization, is equal to the difference between the initial energy of the primary electron and the ionization energy. The total energy is divided in a random way between these two electrons. The electrons are supposed to scatter isotropically in elastic collisions, whereas they are assumed to keep their initial direction of motion after inelastic collisions. The experimental transport cross sections were used for elastic collisions to describe correctly the electron drift velocity.

The choice of the time step is predominantly determined by two factors. First, it is related to the simulation of the elementary processes,[22,23] i.e., an electron can at maximum participate in only one process per time step. Consequently, the time step must be much less than the characteristic time of the process having the largest cross section. Second, it is governed by the errors appearing when the equations of motion for electrons moving in the spatially nonuniform field are numerically integrated. This restriction can be estimated by using the following expression:[24]

$$dt \ll \sqrt{\frac{\langle\varepsilon\rangle D_i}{eL^2\langle v\rangle^3\left(\frac{\partial^2 E}{\partial z^2}\right)_{\max}}}. \tag{8}$$

Here, $\langle\varepsilon\rangle$ is the average electron energy, $\langle v\rangle$ is the average electron velocity, L is the characteristic dimension of the plasma, and D_i is the ion diffusion coefficient. This expression guarantees a good accuracy of the integration of the electron motion equation for the characteristic time of an electron life in the discharge, which is determined by ion diffusion.

It is clear that the superparticle size determines the accuracy and the calculation time, i.e., a large superparticle size (corresponding to a small number of superparticles) results in poor statistics and hence poor accuracy, whereas a small superparticle size (corresponding to a large number of superparticles) results in better accuracy but a long calculation time. We used 16 000–32 000 superelectrons in our calculations.

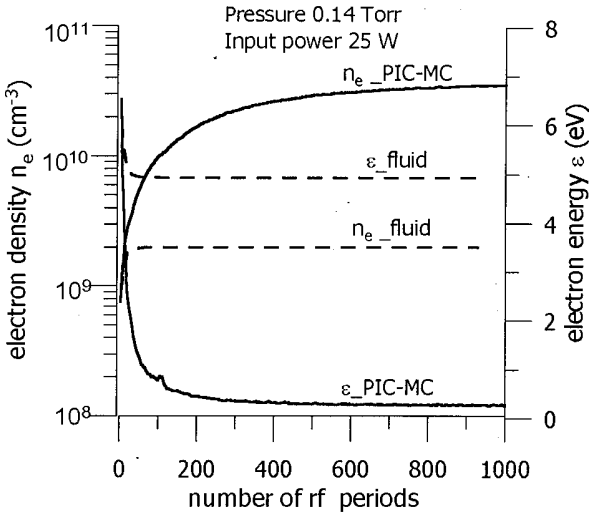

FIG. 1. Time dependence of the electron density n_e and the electron energy ε averaged over a rf cycle in the center of the discharge at a pressure of 0.14 Torr and an input power of 25 W, calculated with the PIC–MC model (solid lines) and the fluid model (dashed lines).

The number of these superelectrons was modified in the algorithm due to ionization processes and loss of superelectrons at the wall. To keep the overall number of superelectrons approximately constant we modified their size and number. If the overall number of the superelectrons exceeded 120% of the required value, then 20% of occasionally chosen superelectrons were ''killed,'' whereas the size of other superelectrons was increased by 25% to keep the overall charge of superelectrons unchanged. If the overall number of the superelectrons reduced to 80% of the required value, then 25% of the occasionally chosen superelectrons were doubled, whereas the size of all superelectrons was decreased by 20%. Superelectron size modification was carried out at a fixed phase of rf discharge. It prevents unwanted switching of this mechanism due to changing of the superelectron number with rf phase.

As mentioned above, at each time step when the superelectrons are followed, the balance equations for the various ions and radicals are also solved, together with Poisson's equation

$$\frac{\partial E}{\partial z} = 4\pi e(n_i - n_e). \tag{9}$$

The potential at the grounded electron is set equal to zero. The potential at the driven electrode is set equal to

$$V(z=L) = -\int_0^L E\,dz = V_{\mathrm{rf}} \sin(2\pi \nu_{\mathrm{rf}} t), \tag{10}$$

where V_{rf} and ν_{rf} are the amplitude and the frequency of the applied potential, respectively. The value of V_{rf} is adjusted until the dissipated power in the discharge equals the electric input power. No dc self-bias voltage is considered in this 1D model.

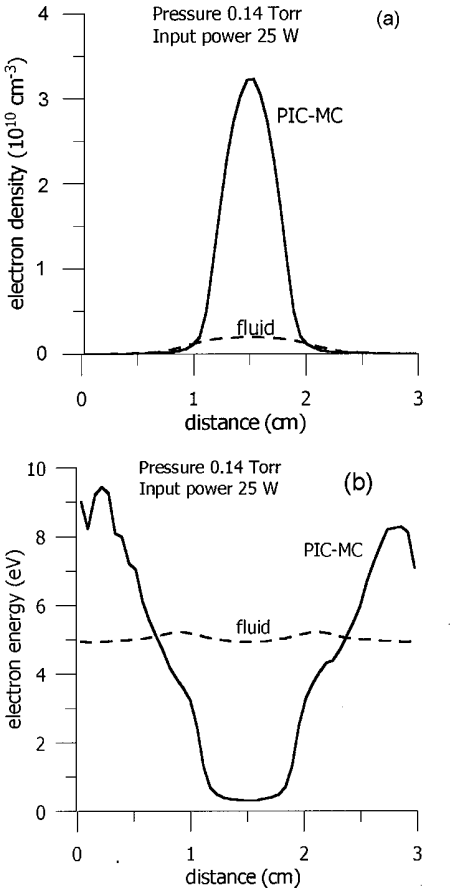

FIG. 2. Stationary state spatial distributions of: (a) the electron density and (b) the electron energy at a pressure of 0.14 Torr and an input power of 25 W, averaged over a rf cycle.

III. RESULTS AND DISCUSSION

The models were applied to an rf discharge in CH_4 at a pressure of 0.14 Torr between two parallel plate electrodes with 20 cm diameter and with interelectrode distance $L=3$ cm. The frequency of the discharge was assumed to be equal to 13.56 MHz. The input power ranged from $P=0.5$ to 25 W. The calculations were carried out until a stationary state was reached. The PIC–MC results were compared with the data calculated by means of the fluid model.

There is an essential difference between the PIC–MC results and the fluid model results at $P=25$ W (calculated discharge current density $j_0=2.2$ mA/cm^2). This is illustrated in Fig. 1, where the electron density and the electron energy averaged over an rf cycle are shown as a function of the number of rf cycles. Whereas the fluid model calculates quasistationary values of the electron density n_e and energy ε after less than 50 rf cycles, the PIC–MC calculation shows a nonstationary character of n_e and ε up to 1000 rf cycles. The difference between the electron densities in the center of the discharge for these two calculations is more than 1 order of magnitude, as appears also from Fig. 2(a). This difference is explained by the formation of a two-temperature bi-Maxwellian EEDF in the center of the discharge in the case of the PIC–MC calculation, which is not calculated by the two-term approximation used in the fluid model. EEDFs at

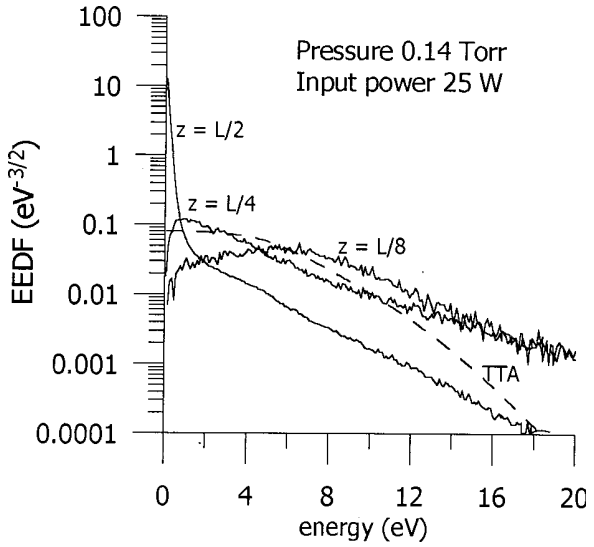

FIG. 3. EEDF at different distances between the electrodes at a pressure of 0.14 Torr and an input power of 25 W, calculated with the PIC–MC model (solid lines) and as a result of solving the homogeneous Boltzmann equation in the two-term approximation, used in the fluid model (dashed line) at an average electron energy of 5 eV.

different distances from the (left) electrode are shown in Fig. 3. The electrons in the discharge can be subdivided into two groups, i.e.: (i) electrons captured in the ambipolar potential eU_a of about 1–2 eV in the center of the discharge, which have no energy input from the oscillating sheaths in the rf discharge and (ii) the other electrons, which can gain energy from the oscillating rf sheaths and are hence characterized by higher energy. The energy input into the low energy electrons decreases when the electron mean free path is greater than the distance between the electrodes. If the energy input into the low energy electrons is smaller than the energy losses, the accumulation of these low energy electrons take place and they form the low energy peak of the EEDF. The electron temperature decreases with increasing electron density, and hence the ambipolar plasma diffusion coefficient decreases. As a result, the so-called ''self-closing'' of the low-temperature plasma is realized, which was considered[24–26] for the case of inert gases. This effect of accumulation cannot be predicted with the fluid model, due to the fact that the ionization rate is then fully determined by the local electric field. The electric field in the center of the discharge cannot be too small and therefore the electron density cannot be too high in the fluid calculations due to the fact that this field actually supports ionization in this region. This is, however, in contrast with reality (as well as with the PIC–MC calculation), where at the pressure of 0.14 Torr the energy relaxation mean free path for ionizing electrons is comparable with the distance between the electrodes. Therefore these electrons can freely move between the electrodes leading to ionization at the center of the discharge, where the amplitude of the electric field is too small to provide the essential ionization rate.

The electron–electron collisions were considered[26] as a mechanism of stabilization of electron accumulation for the case of inert gases. In molecular gases the situation is complicated by the large number of inelastic collisions with low energy thresholds. These collisions lead to increased loss of the electron energy. This effect may considerably increase the value of the pressure at which the accumulation of low energy electrons is possible. Besides, there may be other mechanisms of stabilization of accumulation. In the case of methane, the main energy-loss process for the low-energy electrons is vibrational excitation of CH_4 molecules. As follows from Fig. 1, the stabilization of the average electron energy in the center of the discharge takes place at the level 0.3 eV. This energy corresponds to the maximum in the vibrational excitation cross section of CH_4 and to the Ramsauer minimum in the momentum transfer cross section for CH_4. A further decrease of electron energy in the center of the discharge does not take place since it would lead to a strong drop of energy losses by vibrational excitation and a simultaneous increase of electron heating by the electric field because of the increased momentum transfer cross section.

The superelastic collisions with vibrationally excited molecules might be an additional source of heating for the low-energy electrons. But as follows from an estimation, at the present pressure and electron density, the main process of deactivation of vibrationally excited molecules $CH_4(v)$ is $V-T$ relaxation with a rate constant equal to 2×10^{-14} $cm^3\,s^{-1}$.[27] Hence, the superelastic collisions do not have considerable influence on the heating of low-energy electrons.

In contrast to the results outlined before, we have observed no effect of accumulation of low-energy electrons and a two-temperature EEDF at low input power, $P=0.5$ W ($j_o=0.22$ mA/cm^2). The electron energy has a maximum of ~4.5 eV in the center of the discharge and the results of the fluid and PIC–MC calculations are qualitatively identical (see Fig. 4). The change of the EEDF and the spatial profiles of the electron temperature and density with the value of the input power is very abrupt. Appropriate features of this transition were shown[24–26] for the case of a rf discharge in argon. The accumulation of low energy electrons does not take place at low input power due to the lower electron density in the rf sheath. The thickness of the layer increases at low power and as a result the rf sheaths can overlap and fill the entire interelectrode gap. Hence, there is no region with small electric field values. Joule heating of low energy electrons is greater than their energy losses and accumulation cannot occur. For this reason the quick stabilization of the electron energy and density with time takes also place in the PIC–MC model (see Fig. 5).

The influence of the spatial nonlocality and nonstationarity of the EEDF on the radical production and their fluxes to the substrate is very important from a practical point of view. Spatial distributions of CH_2 and CH_3 radicals calculated with the PIC–MC and the fluid model at $P=25$ W are presented in Fig. 6. It appears that both models give similar values of the radical densities in the discharge gap in spite of the essential differences in the electron density and electron energy in the center of the discharge. This can be explained by the fact that the radical production as well as the ionization are defined by the high-energy part of the EEDF. In Fig. 3, EEDF values are illustrated which are calculated by means

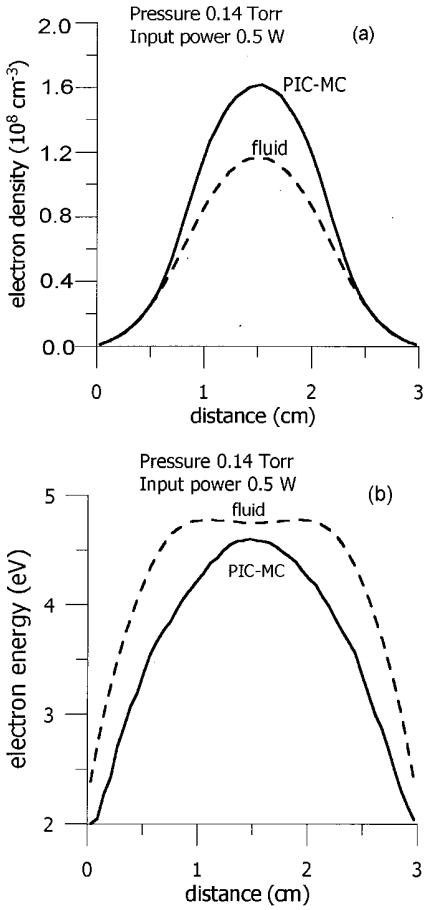

FIG. 4. Stationary state spatial distributions of: (a) the electron density and (b) the electron energy at a pressure of 0.14 Torr and an input power of 0.5 W, averaged over a rf cycle, calculated with the PIC–MC model (sold lines) and the fluid model (dashed lines).

of the PIC–MC model and by solving the homogeneous Boltzmann equation in the two-term approximation (as used in the fluid model) for an average electron energy of 5 eV. This energy is consistent with the stationary value of the average electron temperature in the center of the discharge as calculated in the fluid model. The local EEDF differs considerably from the EEDF calculated by the PIC–MC model at low electron energy, whereas they are rather close at high electron energy. Hence, it is logical that similar radical concentrations are obtained in this case, for the same input power.

IV. CONCLUSIONS

In this article we have presented a 1D PIC–MC model for a capacitively coupled rf discharge in a mixture of CH_4 and H_2. The electron behavior is kinetically simulated by solving Newton's equations and treating the electron collisions with the Monte Carlo algorithm. The behavior of the ions and radicals is treated by a set of continuity equations. The models were applied to a rf discharge in CH_4 at a pressure of 0.14 Torr and a frequency of 13.56 MHz. The PIC–MC results were compared with the data calculated by means of a pure fluid model.[12] An essential difference was

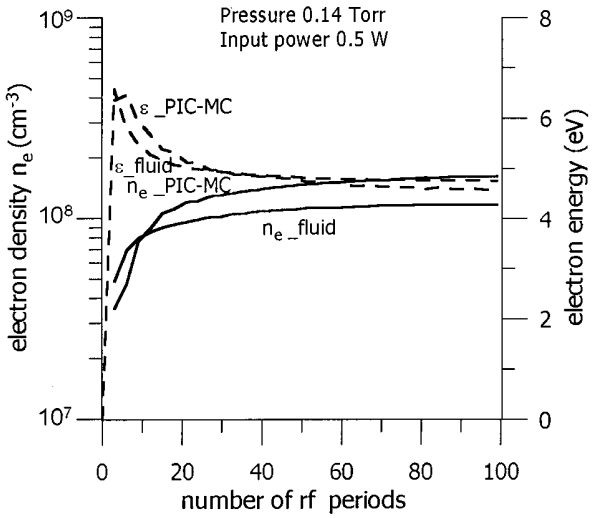

FIG. 5. Time dependence of the electron density n_e and the electron energy ε averaged over a rf cycle in the center of the discharge at a pressure of 0.14 Torr and an input power of 0.5 W, calculated with the PIC–MC model (solid lines) and the fluid model (dashed lines).

observed between the PIC–MC results and the fluid results at an input power of $P=25$ W was found. This difference was explained by the two-temperature bi-Maxwellian EEDF in the center of the discharge in the case of the PIC–MC calculation. The electrons with low energy are captured in the center of the discharge and form the low-energy peak of the EEDF. The other electrons, which can gain energy from the oscillating rf sheaths, are characterized by higher energy. Since the energy relaxation mean free path for ionizing electrons at the pressure of 0.14 Torr is comparable with the distance between the electrodes, these electrons can freely move between the electrodes leading to ionization at the center of the discharge, where the amplitude of the electric field is too small to provide the essential ionization rate. Hence, the EEDF has a nonlocal feature in this case. The effect of

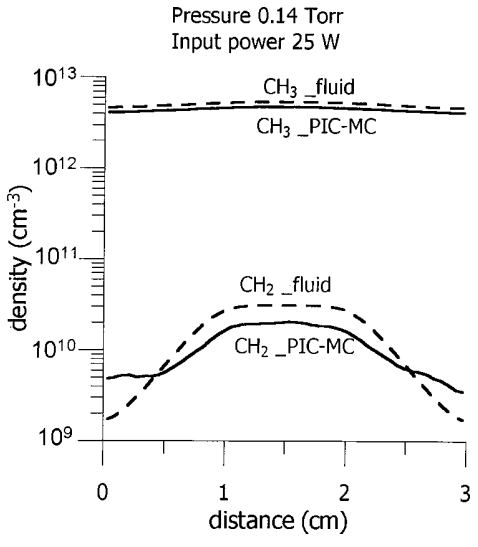

FIG. 6. Stationary state spatial distributions of CH_2 and CH_3 radicals at a pressure of 0.14 Torr and an input power of 25 W.

accumulation cannot be predicted with the fluid model, because the ionization rate is then fully determined by the local electric field. The electric field in the center of the discharge cannot be too small and therefore the electron density cannot be too high in the fluid calculation due to the fact that this field actually supports ionization in this region.

In contrast to the results outlined before, we have observed no effect of accumulation of low energy electrons and a two-temperature EEDF at low input power ($P=0.5$ W). The rf sheath regions overlap and fill the entire interelectrode gap in this case. Hence, there is no region with small electric field values. Joule heating of low energy electrons is greater than their energy losses and accumulation of low energy electrons cannot occur. At this power, the PIC–MC and fluid results are in good agreement.

Finally, the close absolute value and the spatial distributions of CH_2 and CH_3 radicals calculated with the PIC–MC model and th fluid model are also in good agreement. This can be explained by the fact that the radical production as well as electron impact ionization is defined by the high-energy part of the EEDF, which is similar in both models because of equal input power.

ACKNOWLEDGMENTS

This work was supported by NATO's Scientific Affairs Division in the framework of the Science for Peace Program (Project No. NATO SfP 974354) and by the Russian Foundation for Basic Research (Project No. 00-02-16509).

[1] E. Gogolides, D. Mary, A. Rhaballi, and G. Turban, Jpn. J. Appl. Phys., Part 1 **34**, 261 (1995).
[2] E. Dekempeneer, J. Smeets, J. Meneve, L. Eersels, and R. Jacobs, Thin Solid Films **241**, 269 (1994).
[3] K. Tachibana, M. Nishida, H. Harima, and Y. Urano, J. Phys. D **17**, 1727 (1984).
[4] N. Mutsukura, S. Inoue, and Y. Machi, J. Appl. Phys. **72**, 43 (1992).
[5] L. E. Kline, W. D. Partlow, and W. E. Bies, J. Appl. Phys. **65**, 70 (1988).
[6] A. Rhallabi and Y. Catherine, IEEE Trans. Plasma Sci. **19**, 270 (1991).
[7] C. Cavalotti, M. Masi, and S. Carrà, J. Electrochem. Soc. **145**, 4332 (1998).
[8] K. Bera, B. Farouk, and Y. H. Lee, J. Electrochem. Soc. **146**, 3264 (1999).
[9] D. J. Dagel, C. M. Mallouris, and J. R. Doyle, J. Appl. Phys. **79**, 8735 (1996).
[10] M. Masi, C. Cavalotti, and S. Carrà, Chem. Eng. Sci. **53**, 3875 (1998).
[11] A. Von Keudell and W. Möller, J. Appl. Phys. **75**, 7718 (1994).
[12] D. Herrebout, A. Bogaerts, M. Yan, W. Goedheer, E. Dekempeneer, and R. Gijbels, J. Appl. Phys. **90**, 570 (2001).
[13] C. K. Birdsall, IEEE Trans. Plasma Sci. **19**, 65 (1991).
[14] M. Surendra and D. B. Graves, IEEE Trans. Plasma Sci. **19**, 144 (1991).
[15] H. W. Trombley, F. L. Terry, and M. E. Elta, IEEE Trans. Plasma Sci. **19**, 158 (1991).
[16] A. Date, K. Kitamori, Y. Sakai, and H. Tagashira, J. Phys. D **25**, 442 (1992).
[17] V. V. Ivanov, A. M. Popov, and T. V. Rakhimova, Plasma Phys. Rep. **21**, 692 (1995).
[18] V. A. Schweigert, A. L. Alexandrov, S. F. Gimelshein, and M. S. Ivanov, Plasma Sources Sci. Technol. **9**, B1 (2000).
[19] M. Yan and W. J. Goedheer, IEEE Trans. Plasma Sci. **27**, 1399 (1999).
[20] K. Nagayama, B. Farouk, and Y. H. Lee, IEEE Trans. Plasma Sci. **26**, 125 (1998).
[21] A. D. Richards, T. E. Tompson, and H. H. Sawin, Appl. Phys. Lett. **50**, 492 (1987).
[22] T. J. Sommerer, W. N. G. Hitchon, and J. E. Lawler, Phys. Rev. A **39**, 914 (1989).
[23] A. Date, K. Kikamori, Y. Sakai, and H. Tachibana, J. Phys. D **25**, 442 (1992).
[24] V. V. Ivanov, A. M. Popov, and T. V. Rakhimova, Plasma Phys. Rep. **21**, 515 (1995).
[25] V. A. Godyak, R. B. Piejak, and B. M. Alexandrovich, Plasma Sources Sci. Technol. **1**, 36 (1992).
[26] S. V. Berezhoni, I. D. Kaganovich, and L. D. Tsendin, Plasma Phys. Rep. **24**, 556 (1998).
[27] R. M. Siddles, G. J. Wilson, and C. J. S. M. Simpson, Chem. Phys. **188**, 99 (1994).